Diagnostic Techniques for Gaseous Flows 12

A variety of techniques exist that complement or enhance traditional absorption and fluorescence diagnostics. Here we introduce a number of these techniques.

12.1 Absorption Techniques

12.1.1 Frequency-Modulation Spectroscopy (FMS)

In FMS, the optical frequency of a laser is sinusoidally modulated, typically with an electro-optic modulator (EOM), at frequencies equal to or greater than the HWHM of the absorption transition lineshape. This typically requires modulation frequencies from 100 MHz to GHz rates for IR transitions at $\leq$ 1 atm (1 GHz = 0.033 cm^{-1}). The modulation effectively shifts absorption and dispersion information in frequency space to the harmonics of the modulation frequency which lie above lower frequency noise sources. As a result, FMS can provide highly sensitive measurements (down to absorbances of 10^{-8} [1]) of narrow absorption transitions.

Figure 12.1 illustrates a typical experimental setup for an FMS experiment. Frequency modulation is achieved by modulating the voltage applied to an EOM crystal which modulates its refractive index, and therefore, the phase or frequency of the laser beam passing through the EOM. The electric field of the laser beam exiting the EOM is given by:

$$E_o(t) = E_o \exp(i2\pi \nu_c t + i\beta \sin(2\pi f_m t)) \tag{12.1}$$

If the modulation index, β, is < 1, the electric field exiting the EOM predominantly consists of a carrier wave at ν_c and two out-of-phase sidebands located at $\nu_c \pm f_m$, known as a *triplet*. In the absence of wavelength-specific absorption, the triplet is *balanced* and the beat signals (of opposite sign) cancel each other out and go undetected by the photodetector. However, if the triplet is resonant with

R.K. Hanson et al., *Spectroscopy and Optical Diagnostics for Gases*,
DOI 10.1007/978-3-319-23252-2_12

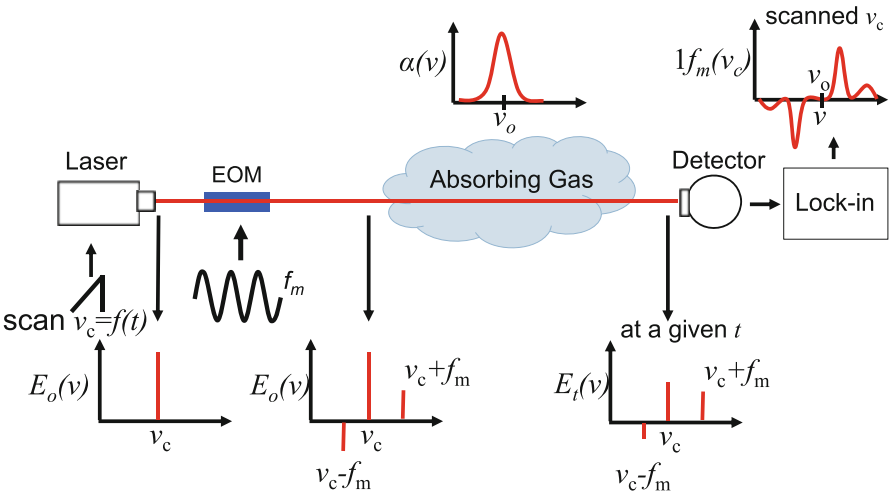

Fig. 12.1 Schematic for laser-absorption measurements using FMS

an absorption transition, the wavelength-specific absorption and dispersion (phase shift) cause unbalance within the triplet (since each component is attenuated and phase shifted a different amount) which introduces a beat signal at f_m in the detector. This beat signal can be extracted via homodyne detection (e.g., with a lockin-amplifier or double-balanced mixer) and compared with measured reference signals or simulated signals to infer gas properties. By scanning the carrier frequency of the laser across an absorption feature, FMS spectra can be measured. More information can be found in [2–6] and the references therein.

12.1.2 Wavelength-Modulation Spectroscopy (WMS)

In WMS, the laser's wavelength is sinusoidally modulated (typically via injection current modulation) about a given location on an absorption transition lineshape (Fig. 12.2). The wavelength modulation leads to intensity modulation, according to Beer's Law, which introduces frequency content centered at the harmonics of the modulation frequency in the detector signal. The harmonic signals can be extracted via lock-in filters during post-processing or data acquisition and can be compared with calibration-free WMS models [7–13] to infer gas conditions (T, P, χ, V) from the measured WMS harmonic signals. Like FMS, WMS enables improved measurement sensitivity via high-frequency modulation, down to absorbances of 10^{-5} [1], but is more versatile than FMS since lower modulation frequencies (f_m is typically 1 kHz to 1 MHz) and larger modulation depths O(0.1–1 cm^{-1}) can be used, the latter of which enables sensitive measurements at high pressures.

$$I_t(t) = I_o(t) \exp[-\alpha(\nu(t), T, P, \chi, L)] \tag{12.2}$$

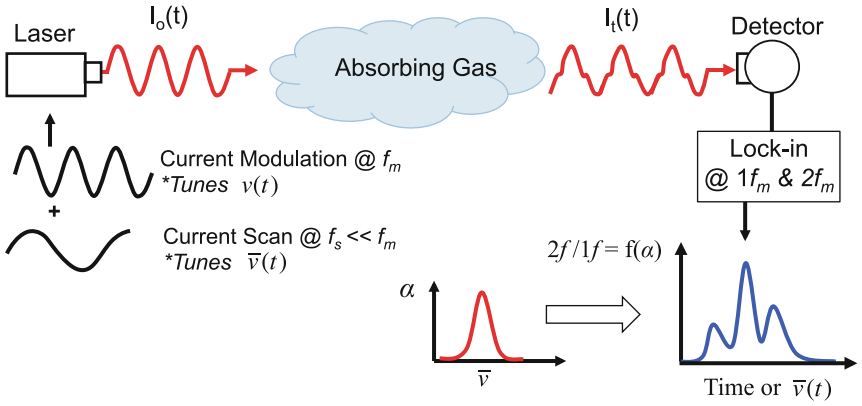

Fig. 12.2 Schematic for laser-absorption measurements using WMS

When using injection-current-tuned lasers (e.g., diode lasers, quantum cascade lasers) the current modulation introduces near-linear intensity modulation that can be exploited to normalize-out the dependence of WMS signals on the DC light intensity and electronic gain [10, 14]. This enables use of first-harmonic-normalized WMS signals that are insensitive to low-frequency (compared to f_m) variations in the light intensity impinging on the detector (e.g., resulting from beamsteering, window fouling, etc.) thereby improving measurement fidelity in harsh environments [10].

12.1.3 Cavity-Ringdown Spectroscopy (CRDS)

Cavity-ringdown spectroscopy enables increased sensitivity in laser absorption detection of a species by increasing the path length over which the light interacts with the absorbing species (Fig. 12.3).

In CRDS, a small fraction of pulsed light is coupled into a cavity through highly reflective mirrors ($R > 99.99\,\%$). This light reflects many times ($> 10{,}000$ passes) so that the light circulating in this cavity has a long interaction path with any gases inside the cavity. The rate of decay of the transmitted intensity can be related to the reflectivity of the mirrors and any other loss processes (e.g., absorption, scattering) of light from the cavity. If a concentration of absorbing species is the dominant loss, the transmitted intensity can be expressed in the following form [15]:

$$I_t(t) = I_o \exp(-t/\tau) \tag{12.3}$$

$$= I_o \exp(-((1-R) + \alpha_{SP}(\nu))ct/L) \tag{12.4}$$

Cavity-ringdown spectroscopy has the potential to be 10,000 times or more sensitive than direct absorption [16]. Variations of pulsed CRDS (Fig. 12.3) include

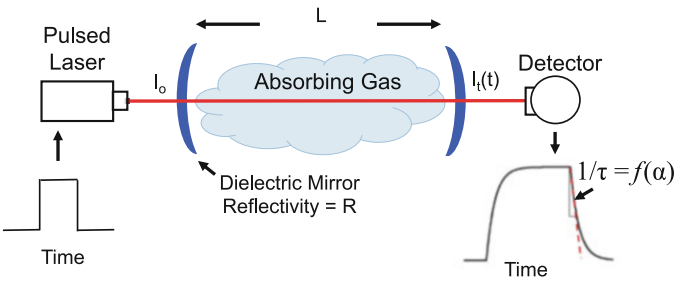

Fig. 12.3 Schematic for laser-absorption measurements using CRDS

CW (continuous wave), PS (phase shift) CRDS, and off-axis integrated-cavity output spectroscopy (OA-ICOS) [17, 18].

For optimum performance, the laser should be coupled into the TEM_{00} mode of the cavity. The spectral width of the laser is also important. If the laser bandwidth is wider than the cavity mode spacing or is not very narrow compared to the absorption linewidth, additional considerations are required [15, 17]. Additionally, a small amount of window fouling can create a significant interference when the beam is reflected from the mirror 10,000 times. Thus, maintaining clean mirrors is critical for sensitive measurements.

12.1.4 Off-Axis Integrated Cavity Output Spectroscopy

Similar to CRDS, OA-ICOS enables improved measurement sensitivity by increasing the effective path length over which light interacts with the absorbing species. However, in OA-ICOS cavity-mode-locking is not required since the reflections within the cavity are spatially separated (laser light travels around the perimeter of the mirrors in an elliptical pattern as it moves back and forth, see Fig. 12.4). At each interface, a small fraction of the light is transmitted through each mirror, and the spatially integrated signal is collected and focused onto a detector. The transmitted intensity exiting the mirror is given by a variant of Beer's Law, Eq. (12.5).

$$I_t(t) = I_o(t)\exp[-\alpha_{CEAS}(\nu)] = I_o(t)/(1 + G\alpha_{SP}(\nu)) \tag{12.5}$$

Here, $I_o(t)$ and $I_t(t)$ are the intensities exiting the cavity in the absence and presence of absorbers, respectively, α_{CEAS} is the effective cavity-enhanced absorbance, α_{SP} is the absorbance for a single pass (i.e., $S(T)P\chi_i\Phi L$), and G is the gain of the cavity.

By spatially separating the reflections, many roundtrips are required before the light rays overlap and retrace their original path through the cavity. The effective cavity length is now m times longer (up to O(1 km)) and the effective free-spectral range (FSR) of the cavity is now m times smaller (typically << HWHM of absorption transition at STP). These attributes enable scanned-wavelength measurements

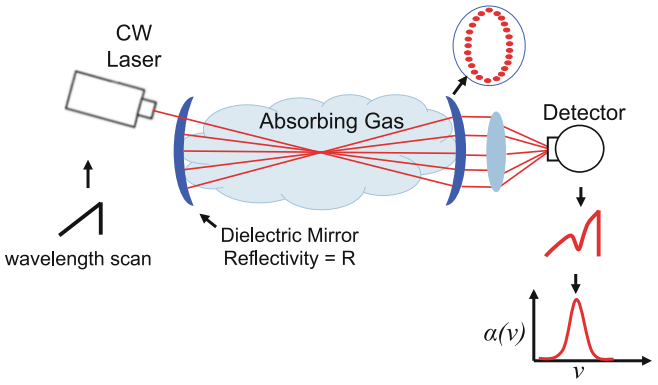

Fig. 12.4 Schematic for laser-absorption measurements using OA-ICOS

of absorption spectra and a cavity-enhanced path length that is much less sensitive to alignment compared to CRDS. More information regarding OA-ICOS can be found in [19–22] and the references therein.

12.2 Fluorescence Techniques

12.2.1 Planar Laser-Induced Fluorescence (PLIF)

One advantage of LIF is that it can easily be extended to two dimensions. By replacing the detector with a 2-D detector array (i.e., a digital camera), and expanding the excitation laser beam into a sheet, a two-dimensional image can be acquired (see Fig. 12.5). PLIF was first applied to combustion in 1982 [23,24]. Details of PLIF can be found in Kychakoff et al. [25] and the extension to high pressure was reported by Lee et al. [26]. PLIF has been used to measure concentration, temperature, pressure, and velocity [27, 28]. Pulsed lasers are normally employed to achieve single-shot imaging, and the short excitation pulse effectively freezes the flow field. While it is useful for measuring quantities in a plane, PLIF can suffer from lower SNR than 1-D LIF because the laser energy is spread out over a much larger area. For steady systems, PLIF measurements may use averaged measurements for improved SNR with either CW or pulsed laser excitation [27, 28].

12.2.2 Narrow Linewidth LIF

Stanford has pioneered the use of rapid-tuning, narrow-linewidth CW lasers for absorption and fluorescence spectroscopy (dye lasers, diode lasers (IR, NIR, VIS)). The LIF linear excitation equation for narrow-linewidth sources is

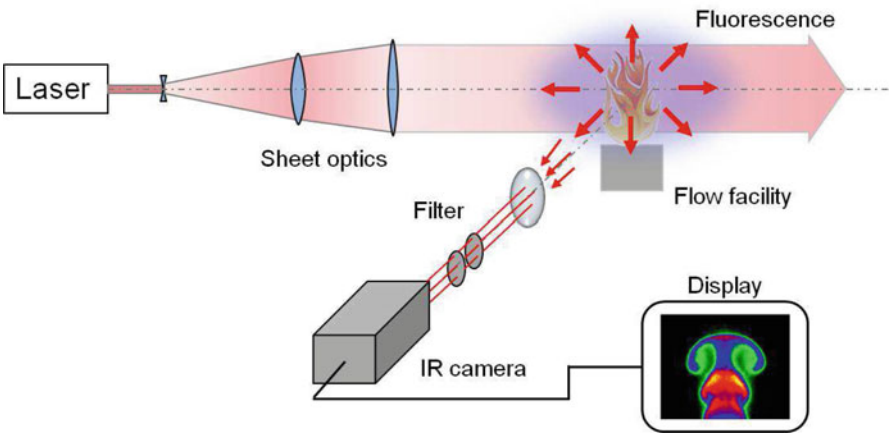

Fig. 12.5 Schematic of a PLIF experiment to measure species concentration

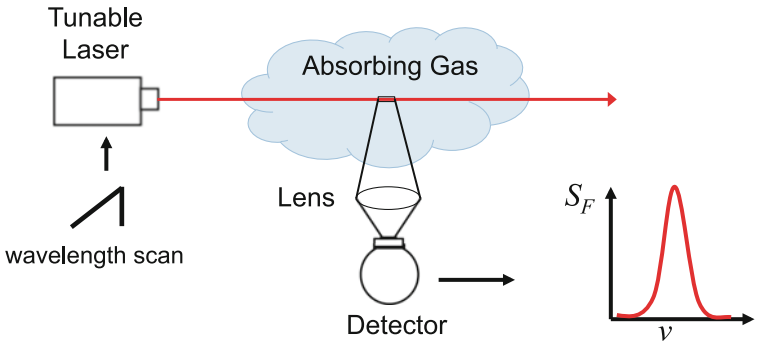

Fig. 12.6 A typical experimental schematic for narrow-linewidth LIF

$$S_F(\nu \rightarrow \nu + d\nu) = n_1^0 \cdot V \cdot \underbrace{I_\nu B_{12}[\phi(\nu)d\nu]}_{W_{12}=\text{prob/s of abs}} \cdot \frac{A}{A+Q} \cdot \frac{\Omega}{4\pi} \tag{12.6}$$

where $\phi(\nu)$ is the absorption lineshape function (see Chap. 8). Recall that $\int \phi(\nu)d\nu = 1$, therefore $\phi(\nu)d\nu$ = the fraction of total probability per second of absorption ($I_\nu\ B_{12}$), for the frequency range $\nu \rightarrow \nu + d\nu$. What can we do with this? We can make spatially resolved measurements of the lineshape function and its integral (Fig. 12.6).

The shape of the LIF line provides opportunities for inferring pressure and temperature, while the integral (area) of the lineshape can provide a measure of $n_1 = n_i f_b(v'', J'')$.

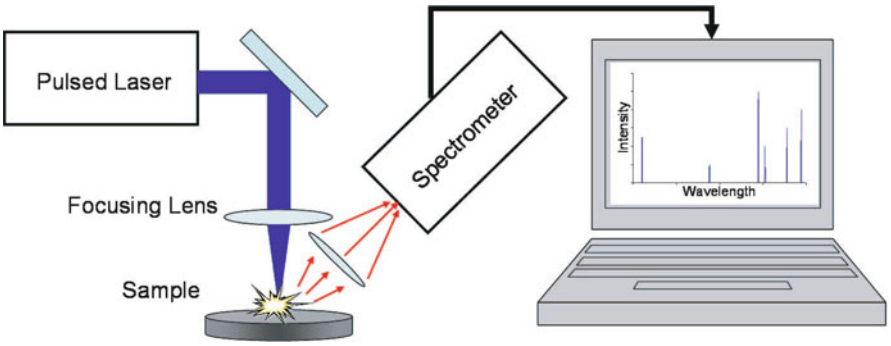

Fig. 12.7 Experimental schematic for LIBS analysis of a condensed-phase specimen

12.2.3 Laser-Induced Breakdown Spectroscopy (LIBS)

Laser-induced breakdown spectroscopy is a simple yet powerful analysis tool for particles and surfaces.

In LIBS, a high-energy laser pulse is focused onto a small sample of unknown composition, ablating a small amount of material from the sample and heating it to high temperatures (∼10,000–20,000 K) [29]. At these high temperatures, the ablated material is broken down into the atoms and ions which constituted the original sample. These atoms emit light at very specific wavelengths, in proportion to the excited-state atomic concentration of the sample. Analysis of the emission spectrum can be used to identify the relative concentrations of the atoms present in the sample, which can then be matched to LIBS spectra of known specimens.

LIBS can be performed on stationary solid or liquid samples as shown in Fig. 12.7 or may be applied to flowing gaseous or particle-laden systems [30, 31]. Variations on standard LIBS include double-pulse and mixed-wavelength systems for enhanced identification [32, 33].

Advantages:
1. Requires little or no sample preparation
2. Can analyze very small sample sizes ($\sim 10^{-9}$ g)
3. Measurement time is typically short (∼1 s)
4. Experimental setup is simple
5. Utilizes high-quality, inexpensive Vis/UV optical components

Disadvantages: LIBS is subject to variation in the pulse energy and can be subject to interference from plasma breakdown of the air surrounding the sample. Quantitative analysis can be complicated by electronic nonequilibrium and unknown, time-varying temperature.

12.3 Photothermal Techniques

Following laser absorption, the upper quantum energy states are depopulated via fluorescence or quenching. LIF is commonly limited by low fluorescence yields, an inefficiency caused by the more dominant quenching process. Conversely, photothermal techniques exploit rapid quenching by relating changes in the translational energy (i.e., temperature) of the gas to the absorbed photon energy. Two variants of photothermal diagnostic methods are presented below.

12.3.1 Photoacoustic Spectroscopy (PAS)

Recall the equation for laser-induced fluorescence signal for the simple two-level model:

$$S_F = (n_2)_{\mathrm{SS}} \cdot A_{21} \cdot h\nu \ \ [\text{energy/vol/s}] \tag{12.7}$$

- Where did the other absorbed energy go? Heating.

$$S_{\text{heating}} = (n_2)_{\mathrm{SS}}\, Q\, h\nu \tag{12.8}$$

$$= n_1^0 \cdot B_{12} I_\nu \cdot \frac{Q}{I_\nu B + A + Q} \cdot h\nu \tag{12.9}$$

$$\approx n_1^0 \cdot B_{12} I_\nu \cdot h\nu \ \ [\text{energy/vol/s}] \tag{12.10}$$

How can we measure the heating strength? Use a pulsed laser and measure the pressure pulse with a microphone! In a confined test cell, where density is constant, the absorbed energy per unit volume is related to the change in temperature and pressure by

$$E_{\text{abs}} = c_v \rho \Delta T \tag{12.11}$$

and

$$\Delta P = \rho R \Delta T \tag{12.12}$$

such that

$$E_{\text{abs}} = c_v (\Delta P / R) \tag{12.13}$$

A cylindrical gas cell may serve as a resonant cavity for sound waves, amplifying the signal when laser modulation is performed at acoustic frequencies. Due to signal dependencies on hardware components, PAS usually requires calibration for

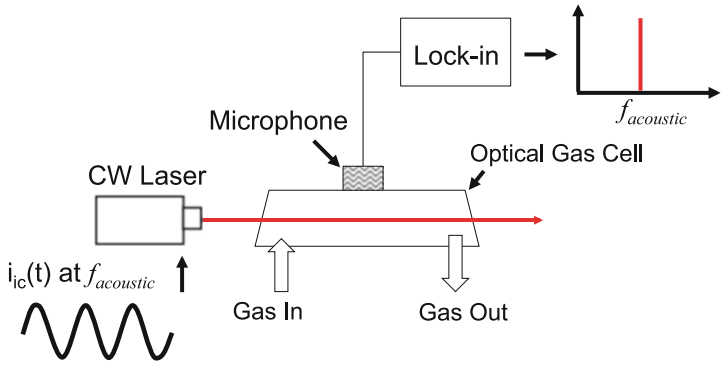

Fig. 12.8 Experimental configuration for optoacoustic measurements

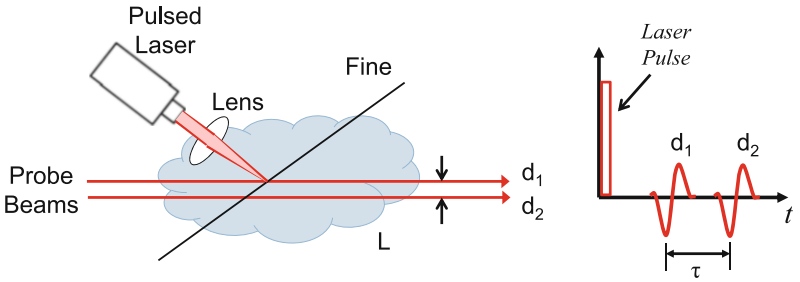

Fig. 12.9 Schematic and data traces for photothermal deflection

quantitative species concentration measurements. PAS is a common technique for species monitoring in relatively quiescent environments (Fig. 12.8).

12.3.2 Photothermal Deflection (PTD)

Temperature from the Speed of Sound

The speed of sound is proportional to $T^{1/2}$, and so a measurement of the speed of a weak pressure wave can be used to infer T. As one example, local heating on a wire from a pulsed laser leads to a pressure pulse that causes deflection of two HeNe probe beams (Fig. 12.9). The times at which the pressure pulse causes deflection at the two different HeNe probe beams is related to their separation distance, L, and the speed of sound in the flow.

$$a = \frac{L}{\tau} \tag{12.14}$$

$$= \sqrt{\frac{\bar{\gamma} RT}{\bar{M}}} \rightarrow T \tag{12.15}$$

An alternative is to use laser spark breakdown to produce a pressure wave.

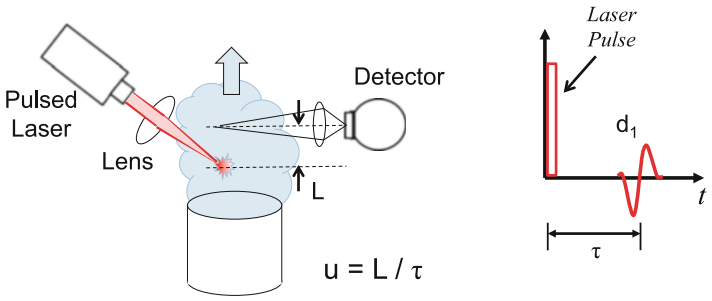

Fig. 12.10 Schematic velocity measurements using photothermal deflection

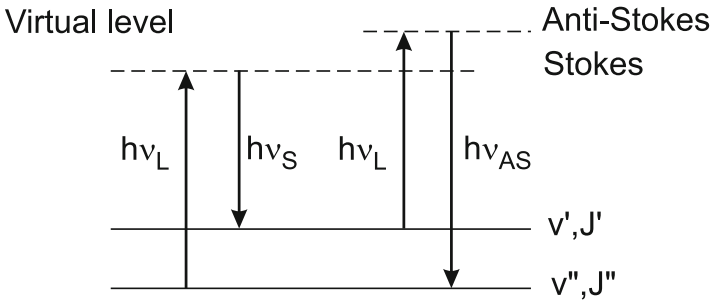

Fig. 12.11 Energy levels for spontaneous Raman scattering

Flow Velocity from Propagation of a Hot Spot

Flow velocity can be inferred from the convection of marked fluid, e.g. a thermal hot spot, as in Fig. 12.10. Alternatively, fluid may be marked by laser excitation to produce a new chemical species or excited state of a constituent species that can be tracked by a probe beam.

12.4 Scattering Techniques

Various forms of spectroscopic detection have been developed based on the Raman effect. Most notable are spontaneous Raman scattering (SRS) and coherent anti-Stokes Raman spectroscopy (CARS).

12.4.1 Spontaneous Raman Scattering

Rotational Raman:	($\Delta v = 0$); changes in J only ($\Delta J = \pm 2$)
Vibrational Raman:	changes in v and J (Fig. 12.11)
Set-up:	Similar to LIF (90° detection); CW and pulsed lasers

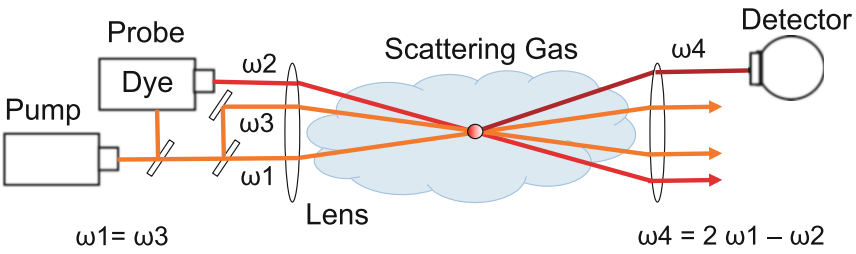

Fig. 12.12 Typical experimental setup for CARS (4-wave mixing)

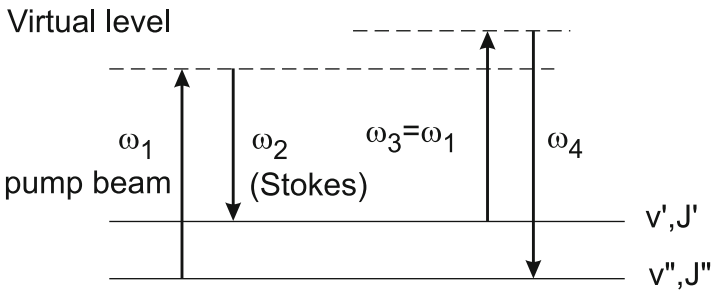

Fig. 12.13 Energy levels for CARS spectroscopy with 4-wave mixing

Uses: measure n_i and T (e.g., by use of filters and $\frac{I_{AS}}{I_S} \propto \exp(-\theta_v/T)$)

$$I(\nu_s) = \frac{cn_i(2J''+1)(v''+1)\exp(-E(v'',J'')/kT)}{Q_{r,v}}(\nu_L - \nu_R)^4 \qquad (12.16)$$

Note: ν^4-dependence favors short-wavelength lasers.

12.4.2 Coherent Anti-Stokes Raman Spectroscopy

Figure 12.12 depicts a typical experimental setup for a CARS experiment and Figs. 12.13 and 12.14 illustrate the energy levels and processes most relevant to CARS. Energy conservation requires that $\omega_4 = 2\omega_1 - \omega_2$, where ω is in frequency units. When $\omega_1 - \omega_2$ is resonant, there is strong, coherent generation of ω_4 via wave-mixing. In addition, conservation of momentum is in effect.

The spectrum and scanning ω_2 mode are depicted in the following figure (Figs. 12.15).

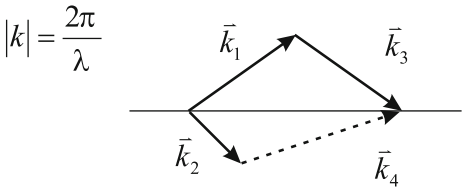

Fig. 12.14 Conservation of momentum for 4-wave mixing

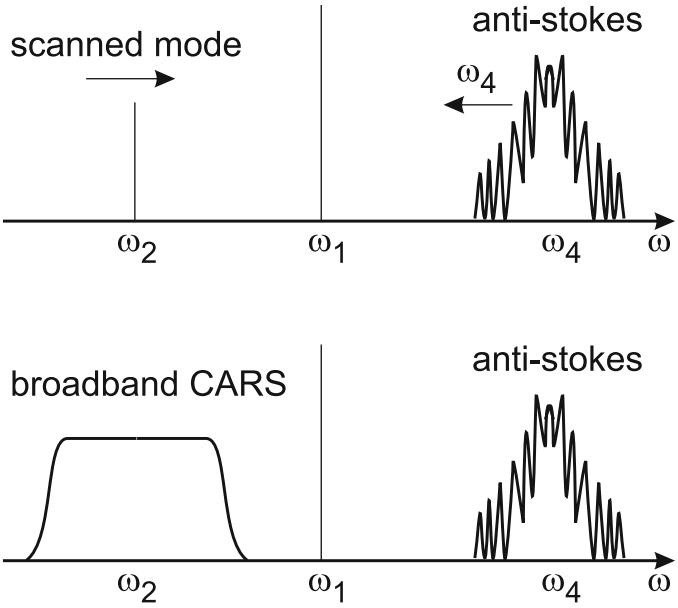

Fig. 12.15 CARS spectra for scanning and broadband sources

Advantages:	directed beam, efficient process
Uses:	thermometry/single shot in jet exhaust
Disadvantages:	complexity of theory/experiment/cost

Modern CARS techniques can provide high temporal and spatial resolution in complex flows [35, 36].

12.5 Laser Ionization Spectroscopy

Multiple analytical strategies have been developed based on the concept of laser-induced ionization (Fig. 12.16).

The lifetimes for laser ionization spectroscopy are as follows:

real levels	$\tau \approx 10^{-9}$
virtual levels	$\tau \approx 10^{-15}$

The experimental schematic for the measurements is shown below (Fig. 12.17).

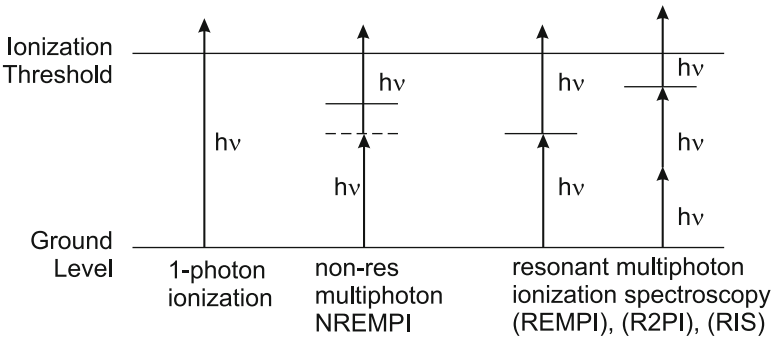

Fig. 12.16 Different energy levels for laser ionization spectroscopy [34]

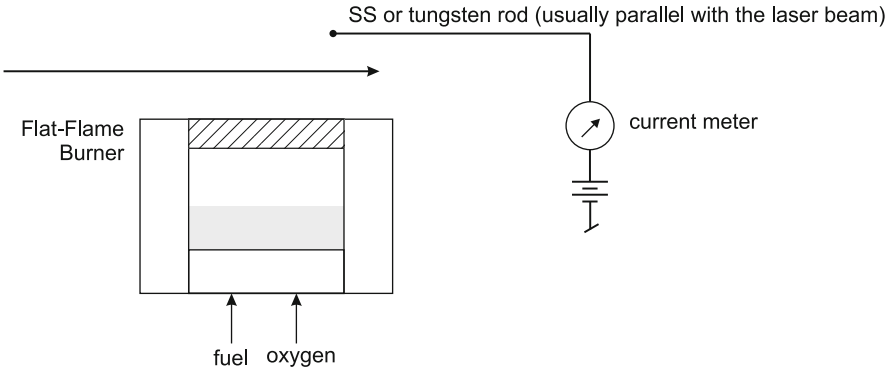

Fig. 12.17 Experimental schematic for laser ionization spectroscopy

Example applications for 3-photon processes:

H-atom detection	$(1S \rightarrow 2S)$ at approximately 121.6 nm
	$2 \times 243 \rightarrow 121.5$ nm
	$2S \rightarrow H^+ + e$ with third photon
O-atom detection	$2^3P \rightarrow 3^3P$
	$3^3P \rightarrow O^+ + e^-$ at 223 nm

References

1. J.A. Silver, Frequency-modulation spectroscopy for trace species detection: theory and comparison among experimental methods. Appl. Opt. **31**(6), 707–717 (1992)
2. G.C. Bjorklund, Frequency-modulation spectroscopy: a new method for measuring weak absorptions and dispersions. Opt. Lett. **5**(1), 15 (1980)
3. G.C. Bjorklund, M.D. Levenson, W. Lenth, C. Ortiz, Frequency modulation (FM) spectroscopy. Appl. Phys. B Photophys. Laser Chem. **32**(3), 145–152 (1983)

4. M. Gehrtz, W. Lenth, A.T. Young, H.S. Johnston, High-frequency-modulation spectroscopy with a lead-salt diode laser. Opt. Lett. **11**(3), 132 (1986)
5. G.E. Hall, S.W. North, Transient laser frequency modulation spectroscopy. Annu. Rev. Phys. Chem. **51**, 243–274 (2000)
6. G. Friedrichs, Sensitive absorption methods for quantitative gas phase kinetic measurements. Part 1: frequency modulation spectroscopy. Z. Phys. Chem. **222**(1), 1–30 (2008)
7. H. Li, G.B. Rieker, X. Liu, J.B. Jeffries, R.K. Hanson, Extension of wavelength-modulation spectroscopy to large modulation depth for diode laser absorption measurements in high-pressure gases. Appl. Opt. **45**(5), 1052–1061 (2006)
8. K. Duffin, A.J. McGettrick, W. Johnstone, G. Stewart, D.G. Moodie, Tunable diode-laser spectroscopy with wavelength modulation: a calibration-free approach to the recovery of absolute gas absorption line shapes. J. Lightwave Technol. **25**(10), 3114–3125 (2007)
9. A.J. McGettrick, K. Duffin, W. Johnstone, G. Stewart, D.G. Moodie, Tunable diode laser spectroscopy with wavelength modulation: a phasor decomposition method for calibration-free measurements of gas concentration and pressure. J. Lightwave Technol. **26**(4), 432–440 (2008)
10. G.B. Rieker, J.B. Jeffries, R.K. Hanson, Calibration-free wavelength-modulation spectroscopy for measurements of gas temperature and concentration in harsh environments. Appl. Opt. **48**(29), 5546–5560 (2009)
11. J.R.P. Bain, W. Johnstone, K. Ruxton, G. Stewart, M. Lengden, K. Duffin, Recovery of absolute gas absorption line shapes using tunable diode laser spectroscopy with wavelength modulation - part 2: experimental investigation. J. Lightwave Technol. **29**(7), 987–996 (2011)
12. K. Sun, X. Chao, R. Sur, C.S. Goldenstein, J.B. Jeffries, R.K. Hanson, Analysis of calibration-free wavelength-scanned modulation spectroscopy for practical gas sensing using tunable diode lasers. Meas. Sci. Technol. **24**(125203), 12 (2013)
13. C.S. Goldenstein, C.L. Strand, I.A. Schultz, K. Sun, J.B. Jeffries, R.K. Hanson, Fitting of calibration-free scanned-wavelength-modulation spectroscopy spectra for determination of gas properties and absorption lineshapes. Appl. Opt. **53**(3), 356–367 (2014)
14. D.T. Cassidy, J. Reid, Atmospheric pressure monitoring of trace gases using tunable diode lasers. Appl. Opt. **21**(7), 1185–1190 (1982)
15. A. McIlroy, J.B. Jeffries, Cavity ring-down spectroscopy for concentration measurements. In *Applied Combustion Diagnostics*, ed. by J.B. Jeffries, K. Kohse-Höinghaus (Taylor & Francis, New York, NY, 2002), pp. 98–127
16. P. Zalicki, Y. Ma, R.N. Zare, E.H. Wahl, J.R. Dadamio, T.G. Owano, C.H. Kruger, Methyl radical measurement by cavity ring-down spectroscopy. Chem. Phys. Lett. **234**(4/6), 269–274 (1995)
17. G. Berden, R. Peeters, G. Meijer, Cavity ring-down spectroscopy: experimental schemes and applications. Int. Rev. Phys. Chem. **19**(4), 565–607 (2000)
18. M. Gupta, T. Owano, D.S. Baer, A. O'keefe, Quantitative determination of the q(1) quadrupole hydrogen absorption in the near infrared via off-axis ICOS. Chem. Phys. Lett. **418**(1/3), 11–14 (2006)
19. A. O'Keefe, Integrated cavity output analysis of ultra-weak absorption. Chem. Phys. Lett. **293**(5–6), 331–336 (1998)
20. A.O. Keefe, J.J. Scherer, J.B. Paul, CW Integrated cavity output spectroscopy. Chem. Phys. Lett. **307**, 343–349 (1999)
21. J.B. Paul, J.J. Scherer, A.O. Keefe, L. Lapson, J.G. Anderson, C. Gmachl, F. Capasso, Bell Laboratories, Lucent Technologies, Mountain Ave, Murray Hill, Infrared cavity ringdown and integrated cavity output spectroscopy for trace species monitoring. **4577**, 1–11 (2002)
22. K. Sun, S. Wang, R. Sur, X. Chao, J.B. Jeffries, R.K. Hanson, Sensitive and rapid laser diagnostic for shock tube kinetics studies using cavity-enhanced absorption spectroscopy. Opt. Express **22**(8), 1–11 (2014)
23. G. Kychakoff, R.D. Howe, R.K. Hanson, J.C. Mcdaniel, Quantitative visualization of combustion species in a plane. Appl. Opt. **21**(18), 3225–3227 (1982)
24. M.J. Dyer, D.R. Crosley, Two-dimensional imaging of OH laser-induced fluorescence in a flame. Opt. Lett. **7**(8), 382–384 (1982)

25. G. Kychakoff, R.D. Howe, R.K. Hanson, Quantitative flow visualization technique for measurements in combustion gases. Appl. Opt. **23**(5), 704–712 (1984)
26. T. Lee, W.G. Bessler, C. Schulz, M. Patel, J.B. Jeffries, R.K. Hanson, UV planar laser induced fluorescence imaging of hot carbon dioxide in a high-pressure flame. Appl. Phys. B Lasers Opt. **79**(4), 427–430 (2004)
27. J.M. Seitzman, R.K. Hanson, P.A. Debarber, C.F. Hess, Application of quantitative two-line OH planar laser-induced fluorescence for temporally resolved planar thermometry in reacting flows. Appl. Opt. **33**(18), 4000–4012 (1994)
28. B. Hiller, R.K. Hanson, Simultaneous planar measurements of velocity and pressure fields in gas flows using laser-induced fluorescence. Appl. Opt. **27**(1), 33–48 (1988)
29. A.C. Samuels, F.C. Delucia, K.L. Mcnesby, A.W. Miziolek, Laser-induced breakdown spectroscopy of bacterial spores, molds, pollens, and protein: initial studies of discrimination potential. Appl. Opt. **42**(30), 6205–6209 (2003)
30. G.A. Lithgow, S.G. Buckley, Effects of focal volume and spatial inhomogeneity on uncertainty in single-aerosol laser-induced breakdown spectroscopy measurements. Appl. Phys. Lett. **87**(1), 11501–11501 (2005)
31. J.P. Singh, H.S. Zhang, F.Y. Yueh, K.P. Carney, Investigation of the effects of atmospheric conditions on the quantification of metal hydrides using laser-induced breakdown spectroscopy. Appl. Spectrosc. **50**(6), 764–773 (1996)
32. D.N. Stratis, K.L. Eland, S.M. Angel, Effect of pulse delay time on a pre-ablation dual-pulse libs plasma. Appl. Spectrosc. **55**(10), 1297–1303 (2001)
33. J. Scaffidi, J. Pender, W. Pearman, S.R. Goode, B.W. Colston, J.C. Carter, S.M. Angel, Dual-pulse laser-induced breakdown spectroscopy with combinations of femtosecond and nanosecond laser pulses. Appl. Opt. **42**(30), 6099–6106 (2003)
34. W. Demtröder, *Laser Spectroscopy: Basic Concepts and Instrumentation*, 2nd enl. edn. (Springer, New York, 1996)
35. S. Roy, J.R. Gord, A.K. Patnaik, Recent advances in coherent anti-Stokes Raman scattering spectroscopy: fundamental developments and applications in reacting flows. Prog. Energy Combust. Sci. **36**(2), 280–306 (2010)
36. C.N. Dennis, C.D. Slabaugh, I.G. Boxx, W. Meier, R.P. Lucht, Chirped probe pulse femtosecond coherent anti-Stokes Raman scattering thermometry at 5 kHz in a Gas Turbine Model Combustor. Proc. Combust. Inst. **35**, 3731–3738 (2015)